

Article

Evaluation of Manning's n Roughness Coefficient in Arid Environments by Using SAR Backscatter

Yuval Sadeh ^{1,*}, Hai Cohen ¹, Shimrit Maman ² and Dan G. Blumberg ¹

¹ Department of Geography and Environmental Development, Ben-Gurion University of the Negev, Beer-Sheva 84105, Israel; haii@bgu.ac.il (H.C.); blumberg@bgu.ac.il (D.G.B.)

² Homeland Security Research Institute, Ben-Gurion University of the Negev, P.O. Box 653, Beer-Sheva 84105, Israel; tiroshs@bgu.ac.il

* Correspondence: yuval.sadeh@monash.edu; Tel.: +61-3-9905-4879

Received: 27 July 2018; Accepted: 14 September 2018; Published: 20 September 2018



Abstract: The prediction of arid region flash floods (magnitude and frequency) is essential to ensure the safety of human life and infrastructures and is commonly based on hydrological models. Traditionally, catchment characteristics are extracted using point-based measurements. A considerable improvement of point-based observations is offered by remote sensing technologies, which enables the determination of continuous spatial hydrological parameters and variables, such as surface roughness, which significantly influence runoff velocity and depth. Hydrological models commonly express the surface roughness using Manning's roughness coefficient (n) as a key variable. The objectives were thus to determine surface roughness by exploiting a new high spatial resolution spaceborne synthetic aperture radar (SAR) technology and to examine the correlation between radar backscatter and Manning's roughness coefficient in an arid environment. A very strong correlation ($R^2 = 0.97$) was found between the constellation of small satellites for Mediterranean basin observation (COSMO)-SkyMed SAR backscatter and surface roughness. The results of this research demonstrate the feasibility of using an X-band spaceborne sensor with high spatial resolution for the evaluation of surface roughness in flat arid environments. The innovative method proposed to evaluate Manning's n roughness coefficient in arid environments with sparse vegetation cover using radar backscatter may lead to improvements in the performance of hydrological models.

Keywords: surface roughness; synthetic aperture radar (SAR); radar backscatter; Manning's n roughness coefficient; hydrological models; arid environment

1. Introduction

Over the last decades, a global increase in the occurrence of floods, the mortality rate and the size of the population affected by floods was reported [1]. In Europe, for example, more people are at risk from floods than a century ago [2]; a large number of these floods are linked by some to climate changes [3], which may in the future even increase flood hazards [4]. Amongst the different types of floods (fluvial, urban and coastal), flash floods are among the most catastrophic disasters, causing the highest number of deaths worldwide [1]. In arid regions, which often suffer from a lack of development, flash floods can be generated in very short time frames; this may be put at risk both human life and infrastructures [5–7]. Therefore, it is essential to acquire information regarding the magnitude and frequency of flash flood events in such areas with the aim of ensuring human life and infrastructure such as bridges and dams. Typically, this information is extracted by using hydrological models. In such models, overland flow generation is reliant upon the simultaneous reaction of numerous variables, including surface roughness. This variable has a marked influence on runoff velocity and depth in that increased surface roughness will lead to reduced runoff velocity

but also to increasingly deep surface detention, which will, in turn, cause high transmission losses [8]. The roughness scale is influenced by the local geology, geomorphology, surface micro-topography and vegetation cover [9–11]. Of particular interest to us are arid environments, which are commonly characterized not only by poor soils, exposed bedrock, low density vegetation cover, high evaporation, and a relatively high rainfall–runoff ratio but also by infrequent low rainfall [5,7,12,13]. The rainfall is often localized and convective, with relatively high rainfall intensities [5,6,14,15].

In hydrological models, surface roughness is expressed by using a hydraulic roughness parameter as a key variable, since surface roughness influences the dynamics and infiltration depth of flood waves, controls the runoff velocity as the runoff flows down the catchment towards the channels, and affects the hydrograph’s timing and peak discharge [11,16,17]. Surface roughness can be estimated using Manning’s roughness coefficient (n) for both overland and channel roughness [10,18,19]. This parameter has found application in flood studies, flood-plain management, and the design of infrastructure, including bridges and roads across flood plains, with a significant number of studies using Manning’s n as input for hydrological models: to mention but a few, Arcement & Schneider [18], El Bastawesy et al. [19], Hernandez et al. [11], Michaud & Sorooshian [9], Semmens et al. [20] and Woolhiser et al. [21].

Manning’s n roughness coefficient is expressed as follows [16]:

$$n = \frac{R^{2/3} S^{1/2}}{V} \quad (1)$$

where R is the hydraulic radius, S is the average slope, and V is the mean velocity of flow (averaged with depth).

Previous studies investigated the potential of integrating hydraulic roughness in the form of Manning’s n and remote sensing data to quantify river discharge [17,22,23]. However, commonly they assigned the Manning’s roughness coefficient based on land-cover/land-use class types interpreted from remote sensing [24–26]. Due to the high influence of vegetation on runoff generation, various remote sensing methods were developed to estimate hydraulic roughness over humid environments using remote sensing, such as using multispectral-based vegetation indices or light detection and ranging (LiDAR) [17,27]. These studies classify the different vegetation types and correlate them to the roughness coefficient. However, the low vegetation cover in arid environments makes it impractical to use most of these approaches in arid regions.

Despite the known importance of the influence of surface roughness on flow characteristics, obtaining spatially detailed hydraulic roughness ground measurements over large areas, such as on a basin scale, is both impractical and expensive [28], especially in arid environments, which are often remote and difficult to access. For this reason, for many years, catchment characteristics were obtained by using point-based measurements. However, a broader picture of surface characteristics can be obtained by applying remote-sensing technologies, which can provide continuous spatial hydrological parameters and variables on a large scale. Among these technologies, spaceborne synthetic aperture radar (SAR) technologies can deliver exclusive information on processes that influence the state and evolution of the Earth’s crust [29]. In particular, data from high-resolution SAR sensors, such as Constellation of Small Satellites for Mediterranean basin Observation (COSMO)-SkyMed, Advanced Land Observing Satellite (ALOS), TerraSAR-X, and RADARSAT-2, can be used to provide improved surface characterization. SAR technologies can also be used to create spatially determined surface roughness maps at a roughness scale closer to the observed scattering [30]. Such extracted roughness data can be used for different applications, including erosion prediction, soil moisture estimations, surface runoff modeling and for estimating the age of desert alluvial surfaces [28,31–33]. However, to the best of the authors’ knowledge, no attempt has been made so far to correlate between radar backscatter and Manning’s roughness coefficient in an arid environment.

Since it was our intention in this study to exploit SAR technology to generate surface roughness maps, let us now take a brief look at the relevant physics of this technology. When radar waves

encounter a rough surface, some of the energy is backscattered and is received by the antenna of a suitably located sensor [34]. Radar backscatter is influenced mainly by the depression and incidence angles, the wavelength, and the polarization of the radiation, the electrical characteristics of the surface materials (which are strongly influenced by water content, expressed as the dielectric constant), the look direction, and the phase difference between the radar waves [35,36]. Properties of natural surfaces, such as roughness, soil characteristics, surface micro-topography, and vegetation cover, also affect radar backscatter [37–39]. The Rayleigh criterion shows that, given constant system parameters (wavelength, incidence angle and flat surface), the backscatter will be a function of the surface roughness on a scale similar to the radar wavelength, i.e., shorter wavelengths are more sensitive to surface roughness [36,40]. In practice, in arid climates, humidity can be taken as constant and, therefore, the radar’s surface backscatter over flat areas (defined as slopes less than 15%) in arid environments is influenced essentially only by the surface roughness [41].

In summary, hydrological models and runoff models, such as KINEROS2, commonly express surface roughness using Manning’s roughness coefficient (n) as the most meaningful surface hydrology roughness parameter. Any improvement in the determination of Manning’s coefficient would obviously significantly enhance such models. The objective of this research was thus to examine whether radar backscatter from spaceborne SAR systems can be exploited to determine Manning’s roughness coefficient by establishing the correlation between radar backscatter and Manning’s roughness coefficient.

2. Methods

2.1. Study Area

The study area comprised the arid, medium-sized (total area of 76 km²) Rahaf watershed, located in the south of the Judean Desert, Israel (Figure 1). The higher western part of the catchment, which is 560 m above sea level, has lower temperatures and a higher mean annual rainfall than the eastern side in the Dead Sea valley, which is 400 m below sea level. The mean annual rainfall on the western and eastern sides of the catchment is 130 mm and 50 mm, respectively. In the Rahaf watershed, the desert lithosoils are shallow, the terrain is governed by exposed Turonian limestone and Senonian chalk bedrocks, and the vegetation cover is very sparse and concentrated mainly along streams. This site was chosen because its surface hydrology has been well studied and documented [15,42,43].

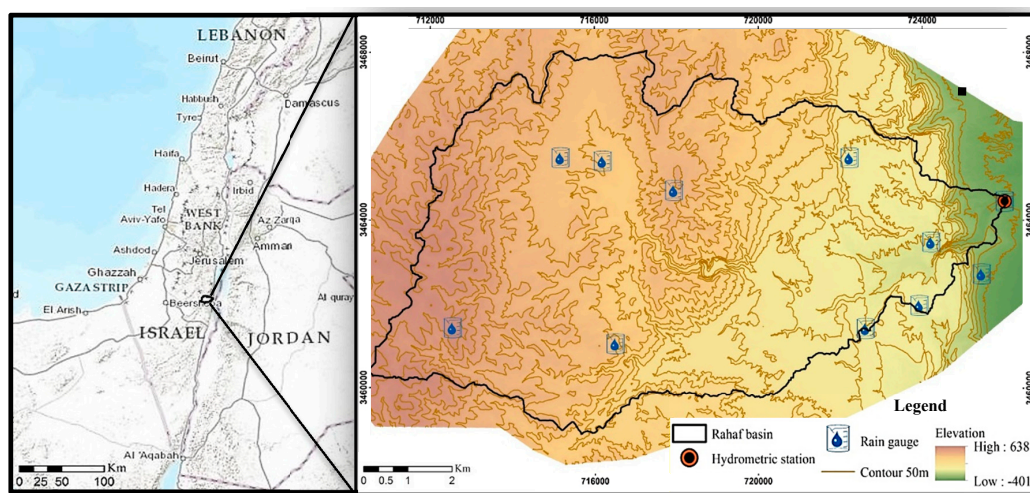


Figure 1. Map of the Rahaf watershed outline by the black line in the enlarged right figure, the rain gauges, and the location of the hydrometric station.

2.2. SAR Data and Processing for Roughness Extraction

COSMO-SkyMed (constellation of small satellites for Mediterranean basin observation) X-band ($\lambda = 3.1$ cm) images were used. The SAR images were acquired on 11 April 2011 using vertical–vertical

(VV) polarization with a 2.5-m spatial resolution (pixel size). The COSMO-SkyMed data were converted to Sigma 0 (dB), rotated, transposed using Environment for Visualizing Images (ENVI) 5.1, and then geometrically corrected using ArcMap 10.2. The final outcome of this process is presented in Figure 2.

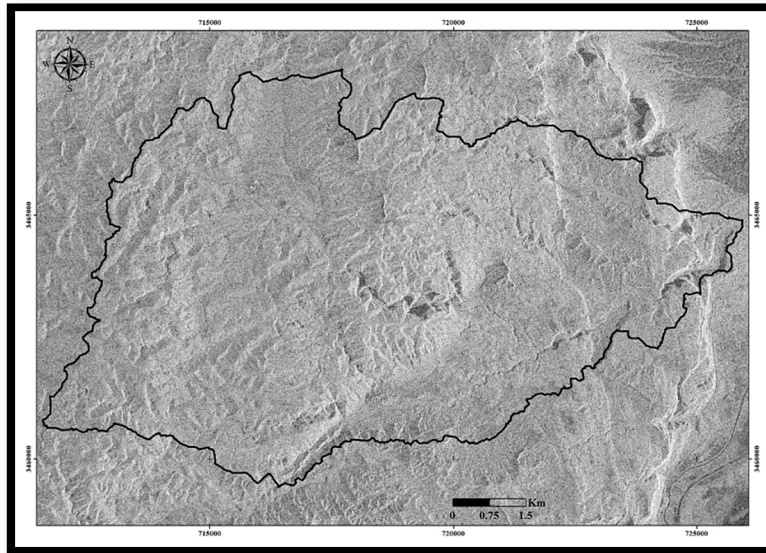


Figure 2. Constellation of small satellites for Mediterranean basin observation (COSMO)-SkyMed synthetic aperture radar (SAR) image of Rahaf basin. Because most of the radar’s energy is reflected away from smooth surfaces, the tone of these surfaces in the image will appear dark, while lighter image tones are caused by the backscatter energy from rougher surfaces back to the antenna [44].

A high-resolution geomorphological map of the Rahaf basin was produced using WorldView-2 multispectral satellite imageries; the results display a high spatial resolution map that classifies the basin into seventeen land cover classes. Of these, 14 are different geomorphological units, two are man-made objects (roads and urban areas) and one contained desert vegetation. As the vegetation cover in our study area is very sparse (only 0.3% of the basin), it was excluded from the subsequent analyses. Although the urban areas and the roads are not geomorphological features, they are important hydrologically. Due to their imperviousness, they tend to produce high volume runoff as the rainfall cannot infiltrate into the soils [3,45]. Next, a number of units suitable for roughness extraction were chosen. As seven of the remaining 16 units in the study area covered less than 2.8% (each) of the region, wide-spread units better representing the geomorphology of the basin were selected. Of the remaining nine units in the study area, six different flat geomorphological units, which cover ~50% of the basin area, were found suitable for roughness extraction. These six units were identified and mapped on the basis of field surveys, a 4-m DEM-based slopes map and WorldView-2 multispectral satellite imageries. For each of the selected geomorphological units, regions of interest (ROI) were sampled with the aim of obtaining the first four statistical moments (average, standard deviation, skewness, and kurtosis) for roughness extraction. Figure 3 shows radar and ground photographs of the six selected units.

2.3. Field Roughness Measurements

Surface roughness in the field can be measured using a variety of different technologies, such as profilometers (sometimes called pinmeters or profilers) [32,46], laser scanners [32,37,47], ground-based LiDAR [48] and airborne LiDAR [49]. In this study, to determine the correlation between the radar backscatter and the surface roughness, the first step was to measure all six geomorphological units in the field with a profilometer, a simple and relatively inexpensive instrument that produces a replica of the surface height variability at 1-cm horizontal spacing. The profilometer used in this study is 1.2 m long (Figure 4). It contains 101 small holes, into each of which is threaded a 1-m long metal rod. The holes are spaced at intervals of 1 cm. The profilometer is connected to two tripods that are used for levelling and

holding the instrument. A plastic board located at the rear of profilometer bears two 30-cm rulers—one on each side—with line scale marks at 1-cm intervals. Although the profilometer is a relatively low-tech instrument for measuring surface roughness, it produces reliable and accurate results and was widely used in previous studies for roughness measurements in the field (e.g., Blumberg & Freilikher [37], Mattia et al. [50], Bryant et al. [46], Alvarez-Mozos et al. [51], and Rahman et al. [28]).

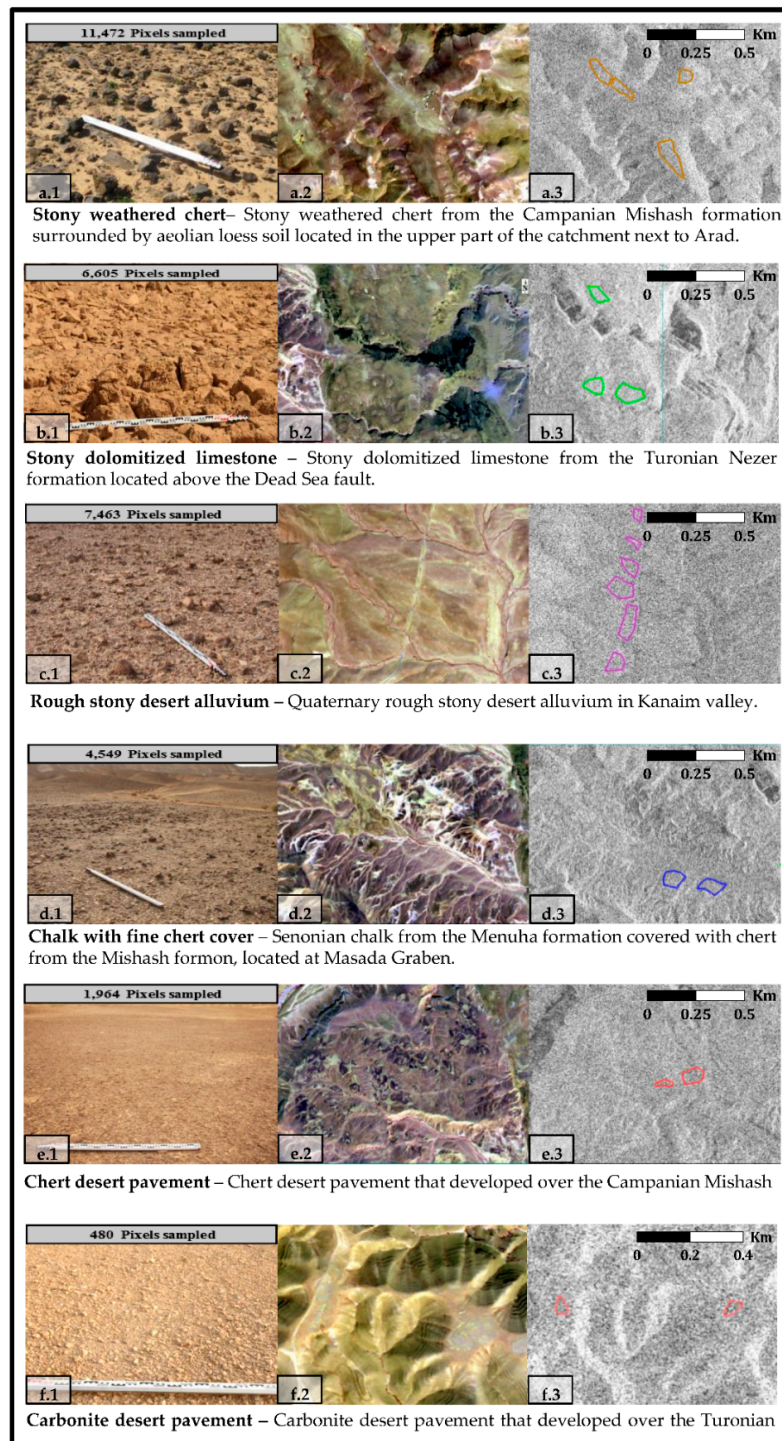


Figure 3. The six geomorphological units and the regions of interest (ROIs) from which the pixels were sampled for roughness extraction (a.1–f.1). The geomorphological unit as photographed in the field and the number of sampled pixels for each unit (a.2–f.2). WorldView-2 image of the ROI region (a.3–f.3). The ROIs used for roughness extraction from COSMO-SkyMed image.

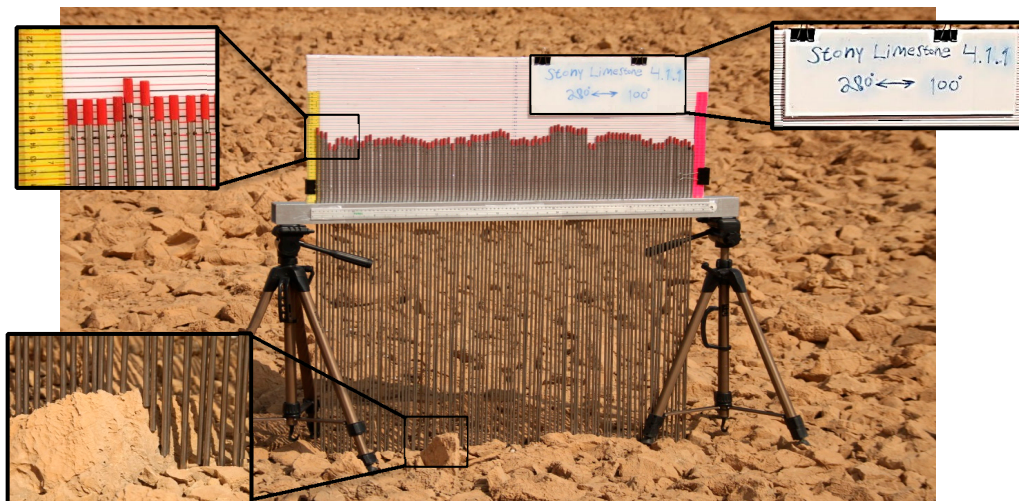


Figure 4. The profilometer as used in the field to measure a stony dolomitized limestone unit. The tips of the 101 rods are colored red to increase contrast from the background. The outcome provides a replica of the surface height variability at 1-cm horizontal spacing.

To obtain the surface roughness from these field measurements, the commonly used root mean square heights (RMS_h) parameter was calculated as follows:

$$RMS_h = \sqrt{\frac{1}{n} \sum_{i=1}^n (z_i - \bar{z})^2} \quad (2)$$

where n is the number of height measurements, z_i is a single measurement, and \bar{z} is the mean of the height measurements [46].

The field roughness measurements (Figure 4) of the six geomorphological units were conducted in five steps as follows: (1) flat surfaces (slopes less than 15%)—without any exceptional micro-topography or unusually large or small stones—that characterize the specific unit were selected; (2) inside the selected area, two 2-m cross strips were measured with a measuring tape; (3) in each 2-m strip, five profilometer measurements were carried out every 50 cm. After positioning the profilometer in place, the rods were threaded into the holes, with the procedure performed gently so as to prevent the rods from penetrating the soil or from moving stones; (4) the properties of the specific measurement were documented on a small board, including the name of the unit, the measurement serial number, and the directionality of the profilometer; (5) roughness measurements were photographed with an SLR camera. The photographs were used for image processing through MATLAB, to extract each rod's height in centimeters, and to calculate the RMS_h.

3. Results

3.1. COSMO-SkyMed Imagery Analysis

The COSMO-SkyMed imagery analysis results, presented in Figure 5, show that the geomorphological unit with the lowest backscatter (expressed in dB) was the carbonate desert pavement unit (−10.63 dB on average), while the highest backscatter values were measured for the stony dolomitized limestone unit (−6.87 dB on average). The standard deviations of the sampled pixels in all the geomorphological units were found to be relatively similar, with values ranging between 5.58 and 5.82 dB.

The skewness values of the sampled pixels in all the geomorphological units were also found to be relatively similar, ranging between −0.91 (carbonate desert pavement) and −1.19 (chalk with fine chert

cover). The lowest kurtosis value of the COSMO-SkyMed sampled pixels was that calculated for the chert desert pavement (1.62), and the highest was the value for the chalk with the fine chert cover (2.81).

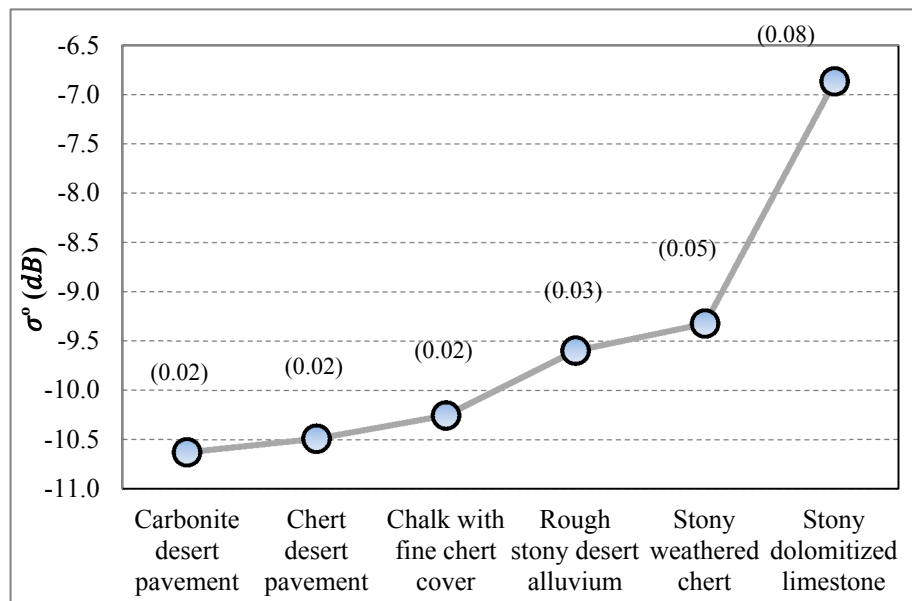


Figure 5. The COSMO-SkyMed average backscatter (dB) of the sampled pixels used to extract the surface roughness of the six selected geomorphological units. In brackets, the Manning's *n* values as determined for each unit based on existing literature and fieldwork.

3.2. Surface Roughness-Field Measurements

The results of the field measurements for surface roughness using the profilometer (expressed as RMS_h) for the six selected flat geomorphological units in the study area showed that the smoothest geomorphological unit was the carbonite desert pavement (RMS_h of 0.82 cm), and the roughest was the stony weathered chert (RMS_h of 1.773 cm). The results indicate that the six units can be roughly divided into three groups: (1) carbonite desert pavement; (2) chert desert pavement and chalk with fine chert cover; and (3) rough stony desert alluvium, stony dolomitized limestone, and stony weathered chert.

Our study area has very few slope features, and because surface roughness is the variable that has the greatest effect on the radar backscatter in flat arid environments [41], one can assume that the variability of backscattering in COSMO-SkyMed imagery did indeed result mainly from the surface roughness. The retrieved results revealed that the smoothest measured geomorphological unit in the study area was the carbonite desert pavement (similar to the field measurements), but—unlike the profilometer measurements—the roughest was the stony dolomitized limestone. We note that the latter unit has an exceptionally high average dB value compared to all the other units (Figure 5). The strong backscatter from the stony dolomitized limestone may be attributed to the micro-topography created by a dolomite “plate-like” geological phenomenon. These plate-shaped dolomites have previously been studied by Raz [52], who described them as brown surface lumps with a diameter ranging between tens and hundreds of meters. Some of them have a topographic depression in the center that is filled with aeolian dust (see location for example: Lat. 31.266781° Long. 35.338309°). Therefore, the strong backscatter is probably related to slopes rather than to roughness. We thus decided to remove this unit from the analysis of the SAR-based data.

3.3. Correlation between the SAR Backscatter and Surface Roughness

An examination of the relationship between the COSMO-SkyMed backscatter and the surface roughness as measured in the field (RMS_h) revealed a strong correlation, $R^2 = 0.97$, when the “problematic” stony dolomite unit was excluded from the analysis (Figure 6).

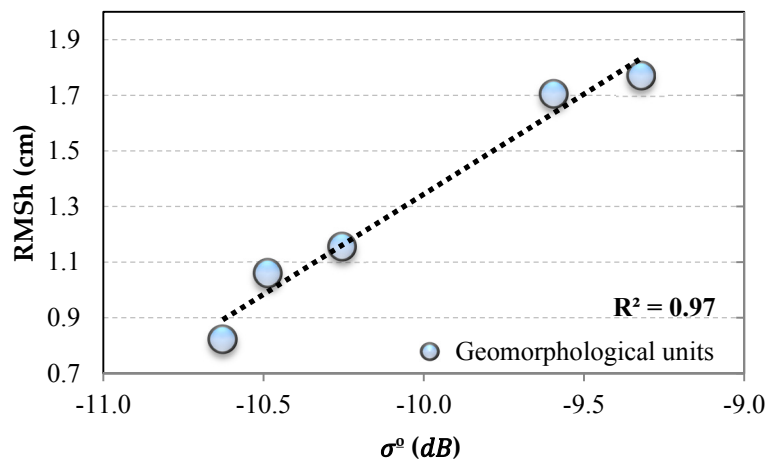


Figure 6. Correlation ($R^2 = 0.97$) between the COSMO-SkyMed backscatter and the surface roughness as measured in the field (root mean square heights (RMSH)).

3.4. Using SAR Backscatter for the Evaluation of Manning’s n

The correlation between the magnitude of the radar backscatter and Manning’s n values for the 16 geomorphological units identified in the study area is shown in Figure 7. This graph also includes the five geomorphological units that were measured in the field and analyzed in this study using COSMO-SkyMed SAR imagery. Manning’s n values for these 16 geomorphological units were determined based on the work of Engman [10], Arcement & Schneider [18], and Woolhiser et al. [21] where equivalent units exist in the literature; the rest were determined based on field judgment experienced expert opinion. In Figure 7, the 16 geomorphological units are ordered according to their roughness level.

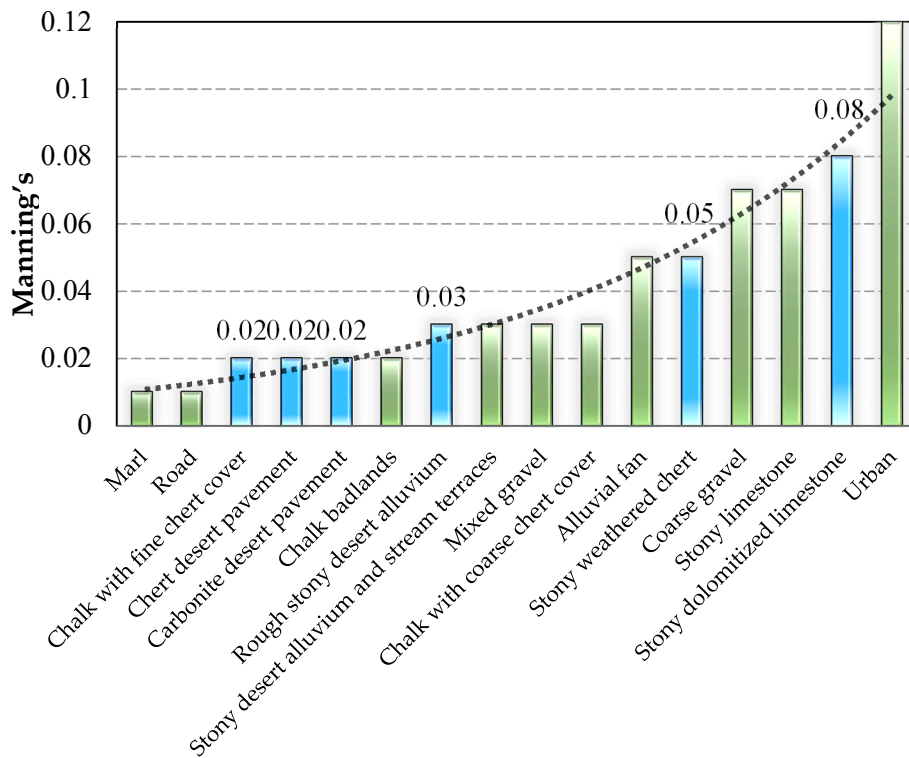


Figure 7. Manning’s n values of the 16 geomorphological units in the study area ordered according to their roughness level. The six geomorphological units that were analyzed using the SAR data are colored in blue.

The results shown in Figure 7 were very satisfactory in terms of the agreement of the positioning of the five units on the graph according to backscatter values and also according to the RMS_h obtained from field measurements and their Manning's n values. Therefore, a schematic diagram, Figure 8, was constructed to evaluate Manning's n values from SAR backscatter (dB) over the study area, even for surfaces for which field measurements were not available.

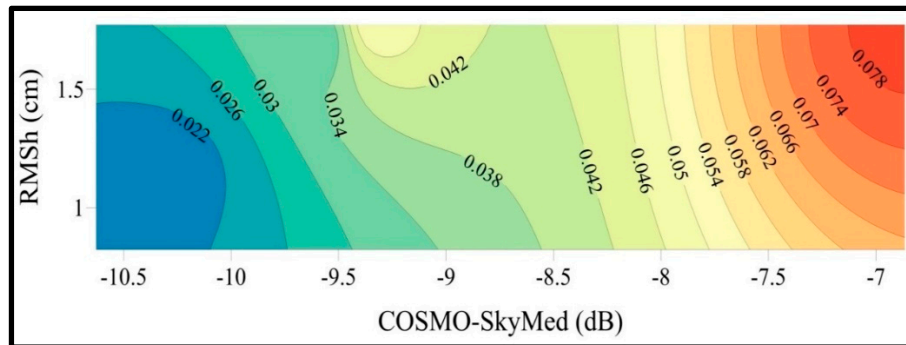


Figure 8. Schematic diagram that enabling the evaluation of Manning's n values by using COSMO-SkyMed backscatter (dB). The blue color in the diagram represents low Manning's n values (smooth surface), and the red color, high Manning's n values (rough surface).

The method used in this study enabled us to create a surface roughness map of the study area, expressed in terms of the Manning's n roughness coefficient, as shown in Figure 9.

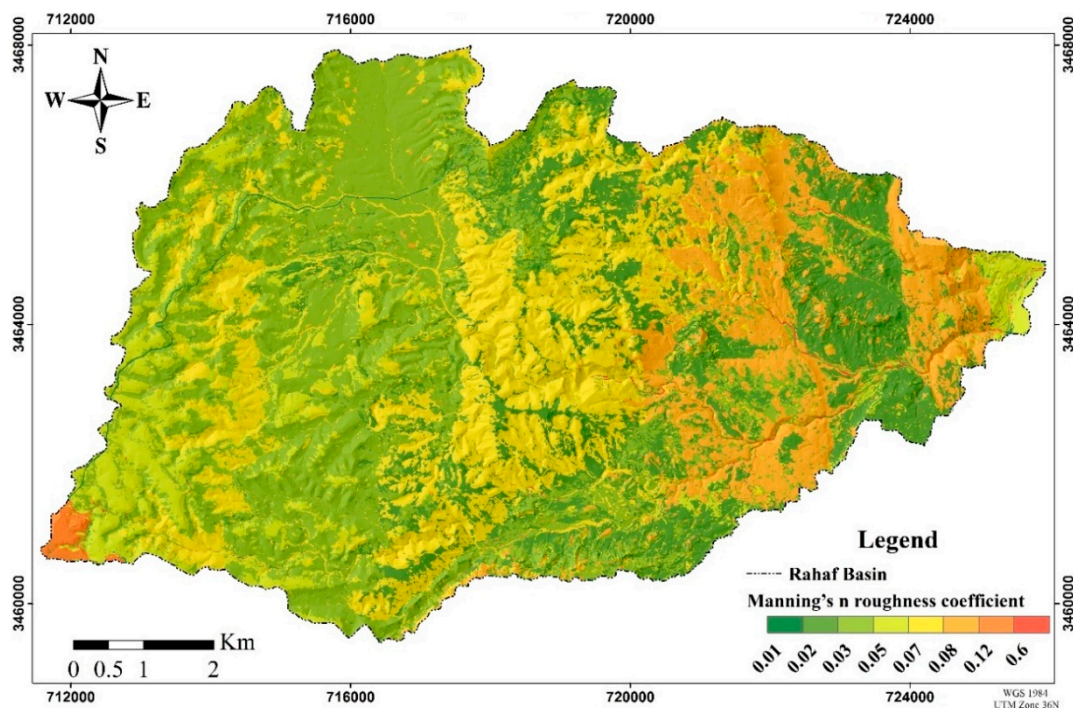


Figure 9. Manning's n roughness coefficient map of the Rahaf basin.

4. Discussion

This study was set to originally estimate the Manning's n roughness coefficient using SAR data. Manning's n is very often used as an input in modeling overland roughness, e.g., Arcement & Schneider [18], El Bastawesy et al. [19], Hernandez et al. [11], Michaud & Sorooshian [9], Semmens et al. [20] and Woolhiser et al. [21], and as such, its extraction is of high importance.

After examining the correlation between radar backscatter and Manning's roughness coefficient in an arid environment, our results suggest that high spatial resolution spaceborne SAR technology can be used to estimate Manning's n roughness coefficient.

The correlation ($R^2 = 0.97$) between the COSMO-SkyMed radar backscatter and the measured surface roughness in the field survey, as shown in Figure 6, illustrates that the novel methodology suggested in this study, which uses radar backscatter as an indicator of the surface roughness in flat arid environments, is indeed suitable for evaluation of surface roughness from X-band COSMO-SkyMed imagery.

The correlation between remote sensing data and Manning's roughness coefficient was studied in the past. Smith et al. [53] showed that airborne remote sensing, such as photogrammetry and LiDAR, has the potential to provide new methods for estimating Manning's n . More recent studies investigating the association between SAR backscatter, roughness, and Manning's n have focused mainly on large floodplains in humid climates. These studies used either airborne SAR (e.g., Horritt et al. [54]) or low spatial resolution spaceborne SAR (e.g., Tarpanelli et al. [55]) to calibrate Manning's n values for channels and floodplains. Mtamba et al. [56] created a Manning's roughness coefficient map based on vegetation classes and Manning's values found in the literature for the large tropical Mara wetland in East Africa. Their map was derived from a Landsat TM-based vegetation map and relative surface roughness from SAR imagery. Unlike previous studies, the technique presented in the current study presents an innovative method using high-resolution spaceborne SAR to evaluate Manning's n in arid landscapes. In contrast to airborne SAR, spaceborne SAR has worldwide coverage and a high temporal resolution and is not affected by weather; it is therefore the preferable technology for such a task.

The correlation between the magnitude of the radar backscatter and Manning's n values for the geomorphological units identified in the study area (Figure 7) shows that the ordering on the graph of the five geomorphological units, whose RMS_h was measured in the field, follows the same pattern as the positions determined by their radar backscattering. Moreover, the order assigned to these five units was the same as that for the Manning's n values. Based on the results, we are confident that an accurate evaluation of Manning's n values could be achieved by using COSMO-SkyMed backscatter (dB), on the condition that the surface sampled in the SAR imagery is flat, dry, and free of vegetation (i.e., conditions commonly characteristic of arid environments). This proposed methodology is highly important in arid environments as they are remote and tend to have low accessibility; therefore, conducting detailed ground measurements of hydraulic roughness over large areas is very difficult and costly.

As Manning's equation is the most commonly adopted approach by engineers to predict runoff generation [54], our method may be relevant in modeling of other types of flooding.

The implementation of our innovative method to estimate Manning's roughness coefficient may also be applicable for evaluating the potential impacts of urban pluvial flooding in urban areas. Urban pluvial flooding, which is also flash in its nature, caused by high intensity rainfall, which go beyond the capacity of the drainage systems [57]. Similar to fluvial flash floods, Manning's n is also used for modelling pluvial flood risks [58]. As the main factors influencing the development of pluvial flash floods are climate changes, rapidly and widespread urbanization and the expansion of unsustainable urban areas [59,60], the importance of rapid large-scale estimations of Manning's roughness coefficient is highlighted. By improving the models' ability to predict regions that are likely to suffer from flooding, engineers may easily identify where flood-defenses need to be built and where to concentrate the efforts in structures reinforcement. However, it is important to note that our method is valid for arid regions with sparse vegetation cover and not for vegetated catchments. Future study should address the question how applicable is this method in regions with denser vegetation cover or in urban areas.

Hydraulic roughness maps have been recognized to be useful for hydraulic modelling [17]. Our method can be used to generate Manning's n roughness coefficient maps of areas of interest similar to the one we created of the Rahaf basin, as shown in Figure 9. The information provided by

such maps can be useful for engineers and hydrologists for planning infrastructure, including bridges and dams, over watersheds. Ideally, this study would have included a comparison of hydrological model performance using, for example, a constant Manning's n in space and a Manning's n allocated using the produced spatially distributed map. Unfortunately, running a hydrological model with variable Manning's values became impossible within the scope of the project; such a sensitivity test will be done in future work. We are confident that our new method may also be used to evaluate the Manning's roughness coefficient for large dry arid streams in addition to arid plains. It may be expected that ongoing advances in spaceborne SAR technology, including in sensors with high spatial resolution, will enable—in the future—a more accurate evaluation from space of Manning's roughness coefficient for most of the streams in catchment areas in arid environments, which can lead to improvements in the performance of hydraulic models.

5. Conclusions

This study used high spatial resolution remote sensing for the hydro-geomorphologic analysis of the Rahaf arid basin. As opposed to previous studies of this nature, which have focused mainly on large humid watersheds, the current research focused on an arid environment and used newly available high spatial resolution spaceborne X-band SAR to estimate surface roughness and to examine the correlation between radar backscatter and Manning's n roughness coefficient.

The results of this study demonstrate a strong correlation ($R^2 = 0.97$) between the COSMO-SkyMed backscatter and surface roughness. It was thus demonstrated that data from an X-band spaceborne sensor with high spatial resolution, such as COSMO-SkyMed, is suitable for evaluating surface roughness in flat arid environments. The correlation between Manning's n values and the SAR surface roughness evaluation enabled us to create a schematic diagram that can be used—instead of field measurements—to estimate Manning's n values for arid plains. Future study may explore the added value of using a Manning's n assigned using a spatially distributed map. It is likely that, as spaceborne SAR technology improves, this method will also be found applicable for evaluating the Manning's roughness coefficient for large dry arid channels and hence lead to improvements in the performance of hydrological models.

Author Contributions: Conceptualization, Y.S. and D.G.B.; Data curation, Y.S.; Funding acquisition, H.C. and D.G.B.; Investigation, Y.S.; Methodology, Y.S. and D.G.B.; Project administration, S.M.; Resources, H.C., S.M. and D.G.B.; Supervision, H.C. and D.G.B.; Validation, Y.S.; Visualization, Y.S.; Writing-original draft, Y.S.; Writing-review & editing, S.M. and D.G.B.

Acknowledgments: The authors thank the Israel Ministry of Agriculture and the Dead Sea Drainage Authority for their support. This project was carried out using COSMO-SkyMed CSK Products, ASI (Italian Space Agency), delivered under an ASI license.

Conflicts of Interest: The authors declare no conflict of interest.

References

1. Hu, P.; Zhang, Q.; Shi, P.; Chen, B.; Fang, J. Flood-Induced Mortality Across the Globe: Spatiotemporal Pattern and Influencing Factors. *Sci. Total Environ.* **2018**, *643*, 171–182. [[CrossRef](#)] [[PubMed](#)]
2. Paprotny, D.; Sebastian, A.; Morales-Nápoles, O.; Jonkman, S.N. Trends in Flood Losses in Europe over the Past 150 Years. *Nat. Commun.* **2018**, *9*, 1985. [[CrossRef](#)] [[PubMed](#)]
3. Kundzewicz, Z.W.; Kanae, S.; Seneviratne, S.I.; Handmer, J.; Nicholls, N.; Peduzzi, P.; Mechler, R.; Bouwer, L.M.; Arnell, N.; Mach, K. Flood Risk and Climate Change: Global and Regional Perspectives. *Hydrol. Sci. J.* **2014**, *59*, 1–28. [[CrossRef](#)]
4. Duan, W.; He, B.; Nover, D.; Fan, J.; Yang, G.; Chen, W.; Meng, H.; Liu, C. Floods and Associated Socioeconomic Damages in China Over the Last Century. *Nat. Hazards* **2016**, *82*, 401–413. [[CrossRef](#)]
5. Yair, A.; Raz-Yassif, N. Hydrological Processes in a Small Arid Catchment: Scale Effects of Rainfall and Slope Length. *Geomorphology* **2004**, *61*, 155–169. [[CrossRef](#)]

6. Singh, R. Real Time Flood Forecasting-Indian Experiences. In *Hydrological Modelling in Arid and Semi-Arid Areas*; Wheeler, H., Sorooshian, S., Sharma, K., Eds.; Cambridge University Press: New York, NY, USA, 2008; pp. 139–156.
7. Foody, G.M.; Ghoneim, E.M.; Arnell, N.W. Predicting Locations Sensitive to Flash Flooding in an Arid Environment. *J. Hydrol.* **2004**, *292*, 48–58. [[CrossRef](#)]
8. Horton, R.E. Erosional Development of Streams and their Drainage Basins; Hydrophysical Approach to Quantitative Morphology. *Geol. Soc. Am. Bull.* **1945**, *56*, 275–370. [[CrossRef](#)]
9. Michaud, J.; Sorooshian, S. Comparison of Simple versus Complex Distributed Runoff Models on a Midsized Semiarid Watershed. *Water Resour. Res.* **1994**, *30*, 593–605. [[CrossRef](#)]
10. Engman, E.T. Roughness Coefficients for Routing Surface Runoff. *J. Irrig. Drain. Eng.* **1986**, *112*, 39–53. [[CrossRef](#)]
11. Hernandez, M.; Miller, S.N.; Goodrich, D.C.; Goff, B.F.; Kepner, W.G.; Edmonds, C.M.; Jones, K.B. Modeling runoff response to land cover and rainfall spatial variability in semi-arid watersheds. In *Monitoring Ecological Condition in the Western United States*; Anonymous; Springer: Berlin, Germany, 2000; pp. 285–298.
12. Greenbaum, N.; Margalit, A.; Schick, A.P.; Sharon, D.; Baker, V.R. A High Magnitude Storm and Flood in a Hyperarid Catchment, Nahal Zin, Negev Desert, Israel. *Hydrol. Process.* **1998**, *12*, 1–23. [[CrossRef](#)]
13. Yair, A.; Kossovsky, A. Climate and Surface Properties: Hydrological Response of Small Arid and Semi-Arid Watersheds. *Geomorphology* **2002**, *42*, 43–57. [[CrossRef](#)]
14. Lange, J. Dynamics of Transmission Losses in a Large Arid Stream Channel. *J. Hydrol.* **2005**, *306*, 112–126. [[CrossRef](#)]
15. Cohen, H.; Laronne, J.B. High Rates of Sediment Transport by Flashfloods in the Southern Judean Desert, Israel. *Hydrol. Process.* **2005**, *19*, 1687–1702. [[CrossRef](#)]
16. Vieux, B.E. *Distributed Hydrologic Modeling Using GIS*, 2nd ed.; Kluwer Academic: Dordrecht, The Netherlands, 2004.
17. Forzieri, G.; Castelli, F.; Preti, F. Advances in Remote Sensing of Hydraulic Roughness. *Int. J. Remote Sens.* **2012**, *33*, 630–654. [[CrossRef](#)]
18. Arcement, G.J.; Schneider, V.R. *Guide for Selecting Manning's Roughness Coefficients for Natural Channels and Flood Plains*; United States Geological Survey Water-Supply Paper 2339; U.S. Geological Survey: Reston, VA, USA, 1989.
19. El Bastawesy, M.; White, K.; Nasr, A. Integration of Remote Sensing and GIS for Modelling Flash Floods in Wadi Hudain Catchment, Egypt. *Hydrol. Process.* **2009**, *23*, 1359–1368. [[CrossRef](#)]
20. Semmens, D.; Goodrich, D.; Unkrich, C.; Smith, R.; Woolhiser, D.; Miller, S. KINEROS2 and the AGWA modelling framework. In *Hydrological Modelling in Arid and Semi-Arid Areas*; Wheeler, H., Sorooshian, S., Sharma, K., Eds.; Cambridge University Press: New York, NY, USA, 2008; pp. 49–68.
21. Woolhiser, D.A.; Smith, R.; Goodrich, D.C. *KINEROS: A Kinematic Runoff and Erosion Model*; Documentation and User Manual; U.S. Department of Agriculture: Washington, DC, USA, 1990.
22. Hagemann, M.; Gleason, C.; Durand, M. BAM: Bayesian AMHG-Manning Inference of Discharge using Remotely Sensed Stream Width, Slope, and Height. *Water Resour. Res.* **2017**, *53*, 9692–9707. [[CrossRef](#)]
23. Pan, F.; Wang, C.; Xi, X. Constructing River Stage-Discharge Rating Curves using Remotely Sensed River Cross-Sectional Inundation Areas and River Bathymetry. *J. Hydrol.* **2016**, *540*, 670–687. [[CrossRef](#)]
24. Thakur, P.K.; Aggarwal, S.; Aggarwal, S.; Jain, S. One-Dimensional Hydrodynamic Modeling of GLOF and Impact on Hydropower Projects in Dhauliganga River using Remote Sensing and GIS Applications. *Nat. Hazards* **2016**, *83*, 1057–1075. [[CrossRef](#)]
25. Ullah, S.; Farooq, M.; Sarwar, T.; Tareen, M.J.; Wahid, M.A. Flood Modeling and Simulations using Hydrodynamic Model and ASTER DEM—A Case Study of Kalpani River. *Arabian J. Geosci.* **2016**, *9*, 439. [[CrossRef](#)]
26. Wang, Y.; Yang, X. Sensitivity Analysis of the Surface Runoff Coefficient of HiPIMS in Simulating Flood Processes in a Large Basin. *Water* **2018**, *10*, 253. [[CrossRef](#)]
27. Forzieri, G.; Degetto, M.; Righetti, M.; Castelli, F.; Preti, F. Satellite Multispectral Data for Improved Floodplain Roughness Modelling. *J. Hydrol.* **2011**, *407*, 41–57. [[CrossRef](#)]
28. Rahman, M.; Moran, M.; Thoma, D.; Bryant, R.; Holifield Collins, C.; Jackson, T.; Orr, B.; Tischler, M. Mapping Surface Roughness and Soil Moisture using Multi-Angle Radar Imagery without Ancillary Data. *Remote Sens. Environ.* **2008**, *112*, 391–402. [[CrossRef](#)]

29. Evans, D.L.; Farr, T.G.; Van Zyl, J.J. Estimates of Surface Roughness Derived from Synthetic Aperture Radar (SAR) Data. *IEEE Trans. Geosci. Remote Sens.* **1992**, *30*, 382–389. [[CrossRef](#)]
30. Verhoest, N.E.; Lievens, H.; Wagner, W.; Álvarez-Mozos, J.; Moran, M.S.; Mattia, F. On the Soil Roughness Parameterization Problem in Soil Moisture Retrieval of Bare Surfaces from Synthetic Aperture Radar. *Sensors* **2008**, *8*, 4213–4248. [[CrossRef](#)] [[PubMed](#)]
31. Marzahn, P.; Ludwig, R. On the Derivation of Soil Surface Roughness from Multi Parametric PolSAR Data and its Potential for Hydrological Modeling. *Hydrol. Earth Syst. Sci.* **2009**, *13*, 381. [[CrossRef](#)]
32. Baghdadi, N.; Paillou, P.; Grandjean, G.; Dubois, P.; Davidson, M. Relationship between Profile Length and Roughness Variables for Natural Surfaces. *Int. J. Remote Sens.* **2000**, *21*, 3375–3381. [[CrossRef](#)]
33. Hetz, G.; Mushkin, A.; Blumberg, D.G.; Baer, G.; Ginat, H. Estimating the Age of Desert Alluvial Surfaces with Spaceborne Radar Data. *Remote Sens. Environ.* **2016**, *184*, 288–301. [[CrossRef](#)]
34. Abdelsalam, M.G.; Robinson, C.; El-Baz, F.; Stern, R.J. Applications of Orbital Imaging Radar for Geologic Studies in Arid Regions: The Saharan Testimony. *Photogramm. Eng. Remote Sens.* **2000**, *66*, 717–726.
35. Blumberg, D.G.; Greeley, R. Field Studies of Aerodynamic Roughness Length. *J. Arid Environ.* **1993**, *25*, 39–48. [[CrossRef](#)]
36. Xia, Z.; Henderson, F.M. Understanding the Relationships between Radar Response Patterns and the Bio-and Geophysical Parameters of Urban Areas. *IEEE Trans. Geosci. Remote Sens.* **1997**, *35*, 93–101.
37. Blumberg, D.G.; Freilikh, V. Soil Water-Content and Surface Roughness Retrieval using ERS-2 SAR Data in the Negev Desert, Israel. *J. Arid Environ.* **2001**, *49*, 449–464. [[CrossRef](#)]
38. Weeks, R.; Smith, M.; Pak, K.; Li, W.; Gillespie, A.; Gustafson, B. Surface Roughness, Radar Backscatter, and Visible and Near-Infrared Reflectance in Death Valley, California. *J. Geophys. Res.* **1996**, *101*, 23077–23090. [[CrossRef](#)]
39. Weeks, R.; Smith, M.; Pak, K.; Gillespie, A. Inversions of SIR-C and AIRSAR Data for the Roughness of Geological Surfaces. *Remote Sens. Environ.* **1997**, *59*, 383–396. [[CrossRef](#)]
40. Campbell, B.A.; Campbell, D.B. Analysis of Volcanic Surface Morphology on Venus from Comparison of Arecibo, Magellan, and Terrestrial Airborne Radar Data. *J. Geophys. Res. Planets* **1992**, *97*, 16293–16314. [[CrossRef](#)]
41. Deroin, J.; Simonin, A. An Empirical Model for Interpreting the Relationship between Backscattering and Arid Land Surface Roughness as seen with the SAR. *IEEE Trans. Geosci. Remote Sens.* **1997**, *35*, 86–92. [[CrossRef](#)]
42. Cohen, H. Floods and Sediment Transport in Dryland Rivers. Ph.D. Thesis, Ben-Gurion University of the Negev, Beersheba, Israel, 2005.
43. Cohen, H.; Laronne, B.J. *Rainfall-Runoff Relations in Arid Environment and Applications for Floods and Sediment Transport Forecast*; Department of Geography and Environmental Development, Ben-Gurion University of the Negev: Beer-Sheva, Israel, 2011.
44. Farr, T.G. *Guide to Magellan Image Interpretation*; Chapter 5: Radar Interactions with Geologic Surfaces; Jet Propulsion Laboratory, California Institute of Technology: La Cañada Flintridge, CA, USA, 1993.
45. Wu, X.; Yu, D.; Chen, Z.; Wilby, R.L. An Evaluation of the Impacts of Land Surface Modification, Storm Sewer Development, and Rainfall Variation on Waterlogging Risk in Shanghai. *Nat. Hazards* **2012**, *63*, 305–323. [[CrossRef](#)]
46. Bryant, R.; Moran, M.S.; Thoma, D.P.; Holifield Collins, C.D.; Skirvin, S.; Rahman, M.; Slocum, K.; Starks, P.; Bosch, D.; Gonzalez Dugo, M.P. Measuring Surface Roughness Height to Parameterize Radar Backscatter Models for Retrieval of Surface Soil Moisture. *IEEE Geosci. Remote Sens. Lett.* **2007**, *4*, 137–141. [[CrossRef](#)]
47. Oh, Y.; Sarabandi, K.; Ulaby, F.T. An Empirical Model and an Inversion Technique for Radar Scattering from Bare Soil Surfaces. *IEEE Trans. Geosci. Remote Sens.* **1992**, *30*, 370–381. [[CrossRef](#)]
48. Mushkin, A.; Sagy, A.; Trabelci, E.; Amit, R.; Porat, N. Measuring the Time and Scale-Dependency of Subaerial Rock Weathering Rates Over Geologic Time Scales with Ground-Based Lidar. *Geology* **2014**, *42*, 1063–1066. [[CrossRef](#)]
49. Turner, R.; Panciera, R.; Tanase, M.A.; Lowell, K.; Hacker, J.M.; Walker, J.P. Estimation of Soil Surface Roughness of Agricultural Soils using Airborne LiDAR. *Remote Sens. Environ.* **2014**, *140*, 107–117. [[CrossRef](#)]
50. Mattia, F.; Le Toan, T.; Souyris, J.; De Carolis, C.; Floury, N.; Posa, F.; Pasquariello, N. The Effect of Surface Roughness on Multifrequency Polarimetric SAR Data. *IEEE Trans. Geosci. Remote Sens.* **1997**, *35*, 954–966. [[CrossRef](#)]

51. Alvarez-Mozos, J.; Gonzalez-Audicana, M.; Casali, J.; Larranaga, A. Effective Versus Measured Correlation Length for Radar-Based Surface Soil Moisture Retrieval. *Int. J. Remote Sens.* **2008**, *29*, 5397–5408. [[CrossRef](#)]
52. Raz, E. The Geology of the Judean Desert. Master's Thesis, The Hebrew University of Jerusalem, Jerusalem, Israel, 1983.
53. Smith, M.; Asal, F.; Priestnall, G. The use of Photogrammetry and Lidar for Landscape Roughness Estimation in Hydrodynamic Studies. *ISPRS XXXB Part B* **2004**, *3*, 714–719.
54. Horritt, M.; Di Baldassarre, G.; Bates, P.; Brath, A. Comparing the Performance of a 2-D Finite Element and a 2-D Finite Volume Model of Floodplain Inundation using Airborne SAR Imagery. *Hydrol. Process.* **2007**, *21*, 2745–2759. [[CrossRef](#)]
55. Tarpanelli, A.; Brocca, L.; Melone, F.; Moramarco, T. Hydraulic Modelling Calibration in Small Rivers by using Coarse Resolution Synthetic Aperture Radar Imagery. *Hydrol. Process.* **2013**, *27*, 1321–1330. [[CrossRef](#)]
56. Mtamba, J.; van der Velde, R.; Ndomba, P.; Zoltán, V.; Mtalo, F. Use of Radarsat-2 and Landsat TM Images for Spatial Parameterization of Manning's Roughness Coefficient in Hydraulic Modeling. *Remote Sens.* **2015**, *7*, 836–864. [[CrossRef](#)]
57. Simoes, N.E.d.C. Urban Pluvial Flood Forecasting. Ph.D. Thesis, Imperial College London, London, UK, 2012.
58. Houston, D.; Werrity, A.; Bassett, D.; Geddes, A.; Hoolachan, A.; McMillan, M. *Pluvial (Rain-Related) Flooding in Urban Areas: The Invisible Hazard*; Joseph Rowntree Foundation: York, UK, 2011.
59. Jiang, Y.; Zevenbergen, C.; Ma, Y. Urban Pluvial Flooding and Stormwater Management: A Contemporary Review of China's Challenges and "sponge Cities" Strategy. *Environ. Sci. Policy* **2018**, *80*, 132–143. [[CrossRef](#)]
60. Acosta-Coll, M.; Ballester-Merelo, F.; Martinez-Peiro, M.; De la Hoz-Franco, E. Real-Time Early Warning System Design for Pluvial Flash Floods-A Review. *Sensors* **2018**, *18*, 2255. [[CrossRef](#)] [[PubMed](#)]



© 2018 by the authors. Licensee MDPI, Basel, Switzerland. This article is an open access article distributed under the terms and conditions of the Creative Commons Attribution (CC BY) license (<http://creativecommons.org/licenses/by/4.0/>).